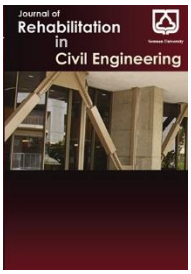

journal homepage: http://civiljournal.semnan.ac.ir/

Seismic Reliability of the Non-Code-Conforming RC Building Due to Vertical Mass Irregularity Effect

Mahdi Adibi[1*], Roozbeh Talebkhah[2]

1. Assistant Professor of Earthquake Engineering, School of Civil Engineering, University of Bojnord, Bojnord, Iran
2. MSc. of Structural Engineering, University of Bojnord, Bojnord, Iran
Corresponding author: *m.adibi@ub.ac.ir*

ARTICLE INFO

Article history:
Received: 08 June 2021
Revised: 13 December 2021
Accepted: 17 December 2021

Keywords:
Vertical mass irregularity;
Fragility curve;
Incremental dynamic analysis;
Existing RC building;
Plain bars;
Seismic reliability.

ABSTRACT

Recent studies showed that the inelastic seismic response of irregular structures can significantly differ from regular structures. Irregular distribution of mass in elevation is regarded as a structural irregularity by which the modes with high energy levels are excited and occasionally prevents the structure from developing nonlinear deformations and causes some unpredictable damages in structural elements. In this study, seismic reliability and risk assessment of a non-code-conforming concrete building reinforced by plain bars is investigated with consideration of the vertical mass irregularity effect. The framework of this study is based on the determination of fragility via incremental dynamic analysis (IDA). The analyses are carried out on a reference 3-story multi-bay 3D structure modeled in Opensees software. Seismic risk assessment for the complete collapse limit state is evaluated by integrating the site hazard and the structural fragility curves. Also, a relatively simple and efficient nonlinear model based on the experimental behavior of substructures reinforced by plain bars is used to simulate pre- and post-elastic behavior buildings. The results indicated that the effects of vertical mass irregularity of the building have almost significant effects on the represented building's fragility curve parameters and seismic reliability of the represented buildings. Probabilities of occurrence for the irregular bottom and median story are about 1.51 and 1.6 times of the building with regular mass distribution.

1. Introduction

One of the irregularities in structures is related to the vertical distribution of the effective (seismic) mass. A different mass distribution in a particular story compared with the adjacent ones can result in the mass irregularity. Because the heavier story requires stronger structural elements, the

How to cite this article:
Adibi, M., Talebkhah, R. (2022). Seismic reliability of the non-code-conforming RC building due to vertical mass irregularity effect. Journal of Rehabilitation in Civil Engineering, 10(4), 14-32.
https://doi.org/10.22075/JRCE.2021.23630.1516

stiffness and strength irregularity may be inevitable. Past studies showed that inelastic seismic response of irregular structures can significantly differ from the regular structures, and their seismic response cannot be precisely assessed by applying the methods used for regular structures. Most of the seismic codes, recommend different analysis procedures for irregular structures, in comparison with regular structures. According to ASCE 7-16 [1], if the effective seismic mass of a story is more than 150% of the effective seismic mass of the adjacent story, the structure has vertical mass irregularity. The Iranian seismic code [2] has similar definitions for vertical mass irregularity and permitted analysis procedures. Also, According to FEMA P-2012 [3], Weight (mass) irregularity tends to reduce collapse resistance, but not dramatically. The location of the mass irregularity along the height of the building moderately affects collapse performance; archetypes with the mass irregularity in lower stories (where the building is already more likely to have damage) tend to have lower collapse capacity than those with mass irregularities in their upper stories.

Many researches have been conducted to investigate seismic response and vulnerability of structures with vertical mass irregularity.

Valmundsson and Nau showed that the elastic response of this type of structures is considerably affected by mass irregularity located at higher stories, whereas inelastic response is affected primarily by mass irregularity located at lower stories [4].

Al-Ali and Krawinkler investigated the effect of vertical irregularities and concluded that in both linear and nonlinear states, mass irregularity insignificantly affected the shear and displacement demands of the structures. Moreover, it was specified that increase in mass of the upper stories, leaves greater effects on the displacement responses of building compared to the case in which lower and middle stories become heavier [5].

Choi showed that mass irregularity is an important factor that affect the response of structures under seismic loading. It was concluded that when the mass irregularity is located at the lower or upper stories, the plastic hinge rotations increase [6].

DeStefano et al. evaluated the irregular RC frames, which had been designed in compliance with Euro-Code 8 (EC-8) to satisfy high ductile requirements. Based on the findings, P-Delta effects could remarkably influence on performance of these buildings [7].

Michalis et al. doubled the mass of several stories in a selected building and conducted an incremental dynamic analysis (IDA) on it. They found that the mass and stiffness irregularities affect the inter-story drifts, considerably [8].

Karavasilis et al. showed that the location of the heavier story and level of inelastic deformation significantly affect the height wise distribution of deformation demands. Generally, the elastic height wise distribution of the deformation demands is uniform, whereas the inelastic one shows concentrations at lower stories. They concluded that the value of the mass ratio (the ratio of the heavier mass to the mass of an adjacent story) does not influence roof drift, interstory drift and rotation ductility demands. On the other hand, deformation demands are influenced by the location (bottom, mid-height or top) of the heavier story [9].

Pirizadeh and Shakib pointed out that the seismic performance of structures can be significantly affected by the location of mass irregularity. They showed that if the heavier story was located at the bottom half of an eight-story steel structure, the return periods of the structures would exceed the collapse prevention and performance level of global instability would decrease compared with

those of a regular structure [10]. In similar research, Habibi and Asadi studied on Seismic Performance of reinforced concrete frames by considering effects of vertical irregularity Based on Iranian Seismic Code [11].

Mohsenian and Nikkhoo studied the effects of vertical mass irregularity on seismic performance of RC tunnel-form structural system. The results indicated that the pattern of mass irregularity does not affect the location of first damages induced by the DBE hazard level. Also Irregular distribution of mass in height increases the fundamental period, as well as coefficient of mass contribution of the primary vibration modes [12].

Amiri and Yakhchalian studied the effects of intensity measures on seismic collapse assessment of structures with vertical mass irregularity. The results show that the scalar value of Sa_{avg} satisfies the desired features of an optimal IM to predict the collapse capacity of low- and mid-rise steel SMRFs with vertical mass irregularity. Therefore, the fragility functions obtained using these optimal IMs are more reliable for this type of structures [13].

Karami et al. studied on the effects of vertical mass irregularity on Seismic Behavior of high-rise steel frames with buckling-restrained braces. Results are shown, mass irregularity increase the values of maximum drift, floor acceleration and top floor displacement [14].

Ghimire and Chaulagain studied on seismic performance of RC frame buildings by influence of structural vertical irregularities. Results are shown mass irregularities considerable effects on seismic response of RC frames [15].

Bai et al. studied on the shaking table test of low-rise steel moment frames by considering effects of mass irregularity. Results are shown, the specimen with the mass irregularity on the top storey considerable increase the drift responses when subjected to over-design earthquakes [16].

In the present study, an existing non-code-conforming 3-story concrete building reinforced by plain bars with and without vertical mass irregularity were modeled and analyzed under incremental dynamic analysis by considering beam-column joint effects. Concrete buildings reinforced by plain (smooth) bars are one of the special types of old reinforced concrete buildings. They were generally built before the 1970s and some of the older cases were probably designed just for gravity loads [17] and do not have special seismic detailing for structural members because the old building codes did not include special seismic provisions at that time [18]–[21]. The results of our previous experimental research have shown large damages especially at the beam–column joints caused by bar slippage and moment capacity of the adjacent beam controls nonlinear behavior of substructure. Beam-column joints was simulated by a model developed in our previous research [22].

The goal of this study is to understand the effects of vertical mass irregularity on collapse capacity of the existing RC building with plain bars. To achieve this goal, the mass ratio of 1.5 was considered as the limit of vertical mass irregularity. Also, effect of location of vertical mass irregularity at the lower or upper stories on collapse capacity were investigated. The analysis procedure conducted in this study are summarized in a flowchart as shown in Fig. 1. Incremental dynamic analyses (IDA) of the existing 3-story building with plain bars were conducted to propose fragility curves parameters at collapse damage states. In IDA, a structural model is subjected to a set of ground motion records, scaled to different levels of intensity to describe the structural behavior from elastic to collapse [23].

IDA was then conducted along both E-W directions and N-S directions. These IDA curves were obtained from a series of

nonlinear time history analyses when each of the 20 selected ground motions that included two horizontal components were applied to the 3D building models at increasing intensity.

A damage state is defined as a threshold condition of buildings corresponding to a certain level of damage under an earthquake [21]. So, HAZUS-MH-MR-5 provisions was used to determine damage limit states [24].

Fragility curves demonstrate the probability of building damage for various levels of earthquake intensity. Each point on the fragility curve shows the probability of exceeding a specific damage limit state under an earthquake with a given intensity [25]–[28].

Seismic reliability of the represented structure was evaluated by integrating site hazard and structural fragilities resulting for complete collapse limit state [29], [30].

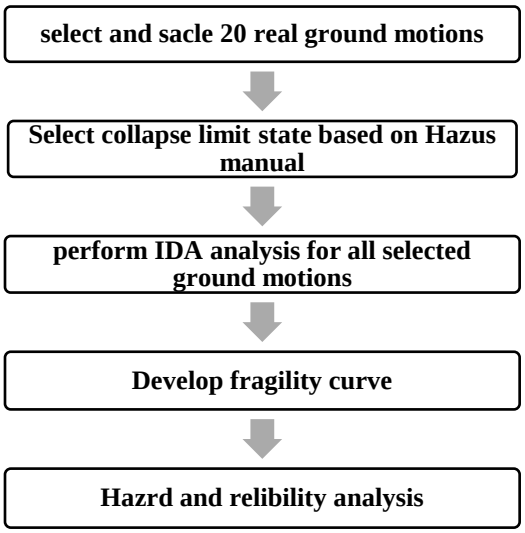

Fig. 1. Analysis procedure for Seismic fragility and reliability of existing RC building with plain bars.

2. Properties of representative buildings

In this study, seismic behavior of non-code-conforming and existing concrete building reinforced by plain bars with 3 stories was investigated. The represented buildings are considered to be isolated from an existing three-story residential RC building built prior to the 1970s [31]–[36]. It is easy to find a lot of old buildings with the same details in other countries such as Italy, Portugal and Turkey according the old design codes and references [31]–[36] In this regard, geometrical and detailing information of surveyed typical RC buildings constructed prior to the 1970s was taken into account.

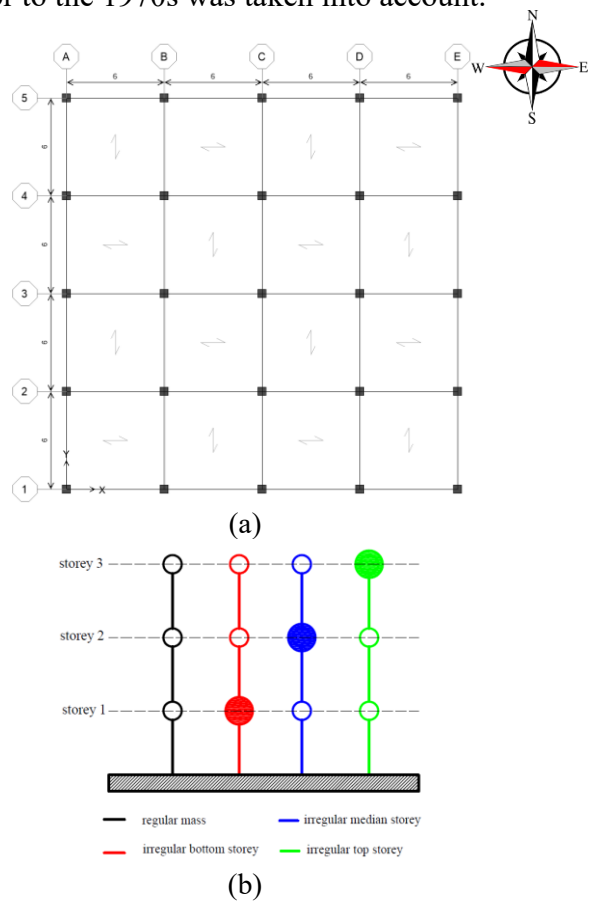

Fig. 2. Plan and Irregularity mass patterns of selected buildings (dimension in meters).

The story height and effective beam span length are 3 m and 5.5 m, respectively. The plan view of the building was shown in Fig. 2(a). Fig. 2(b) shows the mass distribution of the stories in the regular and irregular structures. In this study, the limit state of the

mass ratio of stories was considered to investigate the effect of mass irregularity on the seismic performance of the structure. Most of the seismic codes [1], [2] represented the mass ratio of 1.5 as the limit of vertical mass irregularity.

Dimensions and reinforcement details of the beams, columns and, connections of the buildings represented in this study were shown in Fig. 3. All the beams and columns in the represented building have similar dimensions and reinforcing details. The cross section dimensions of the columns and beams were 250×250 mm and 200×300 mm, respectively. Regarding the reinforcement, 4Φ14 (ρ_{col} = 1%), and Φ6.5@160mm plain bars were used respectively for longitudinal and transverse reinforcement of the column. The compressive strength of the concrete and the yield strength of the reinforcing bars were 21 and 340 MPa, respectively. The abbreviation of (RCP) was assigned to the regular concrete building reinforced by plain bar. Also, abbreviations of (IRCP-B), (IRCP-M) and, (IRCP-T) were assigned to the concrete building reinforced by plain bar with mass irregularity located at bottom, medium and top story, respectively.

The natural periods corresponded to the first mode of the RCP, IRCP-B, IRCP-M and IRCP-T buildings are 0.478 sec, 0.483 sec, 0.504 sec and 0.514 sec, respectively.

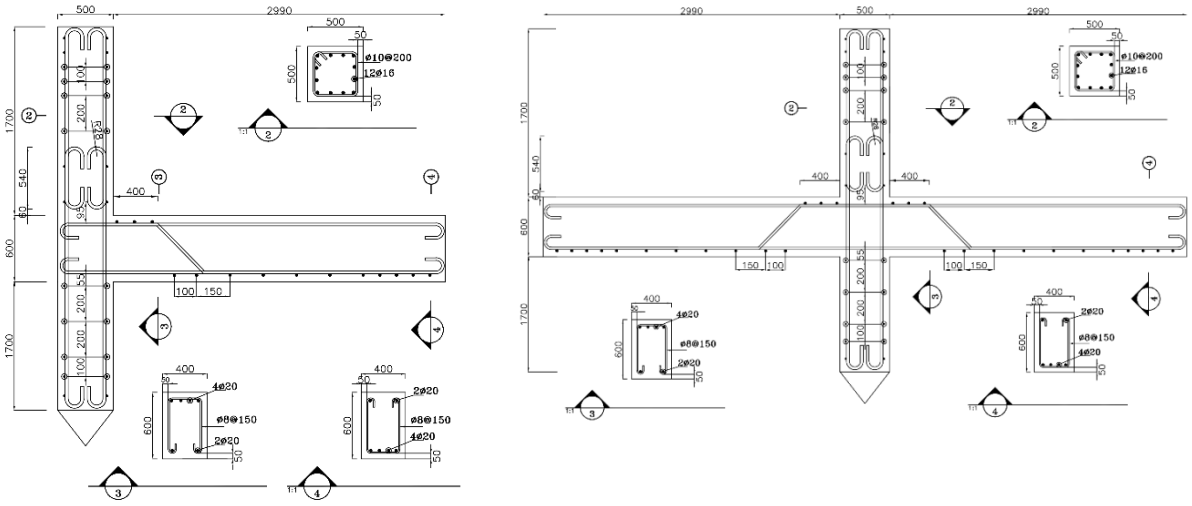

(a) exterior joint. (b) interior joint.

Fig. 3. Detailing of the beam-column connection [22].

3. Nonlinear simulation methodology

For dynamic analyses of the buildings, a three-dimensional model was created in Opensees software [37]. P-Delta effects were considered in the numerical model and the floors were simulated by rigid diaphragm. Also, 5% Rayleigh damping were considered in the numerical model [38], [39]. Norm Displacement Increment test was used for convergence algorithm. Newton algorithm specify the steps taken to solve the nonlinear equation. Also, integrator Newmark was used in Transient Analysis of the model. In this study, nonlinear behavior of beam-column joints were simulated by a nonlinear model proposed by Adibi et al.[22]. Also, some experimental works on the exterior and interior joint substructures reinforced by

plain bars were performed to confirm the numerical model represented in this study [19] [20] [22]. Due to the cracking pattern observed in the substructure (Fig. 4), it can be assumed that the nonlinear behavior of the section at the end of the beams controls the nonlinear behavior of the substructure. Therefore, a nonlinear rotational spring was considered at the end of the beam and at the connection to the column for introducing the nonlinear behavior of the substructure (Fig. 5). According Fig. 4, the substructure was mainly damaged at the end of the beam (intersecting with the joint panel zone), so panel zone modeled by rigid elements and beam and column modeled by Linear Beam-Column elements. The final parameters assigned to the nonlinear rotational spring can be seen in Fig. 6. Pinching 4 constitutive model available in the library of the Opensees software was employed to define nonlinear behavior of the spring at the critical section of the beam.

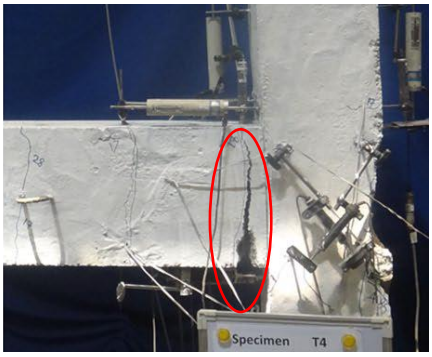

a) Exterior joint.

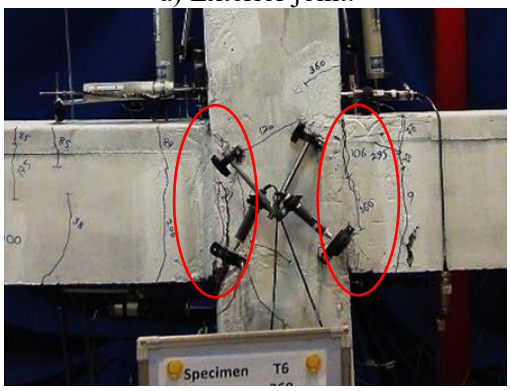

b) Interior joint.

Fig. 4. Damage progression and crack observation for the interior and exterior substructure at drift 2.7% [22].

Yield rotation [22][40][41] can be calculated by Eq. (1) and the nonlinear values of the rotational spring had been calibrated by experimental behavior of the studied specimens, which is presented in Table 1.

$$\theta = \frac{M \; L_b}{E \; I_b} \tag{1}$$

Where M, L_b, E, I_b, are flexural moment, length, modulus of elasticity and moment inertia of the adjacent beam, respectively.

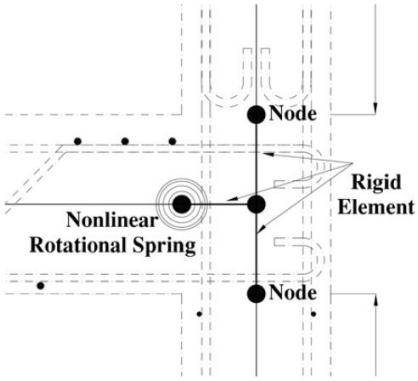

a) Exterior joint.

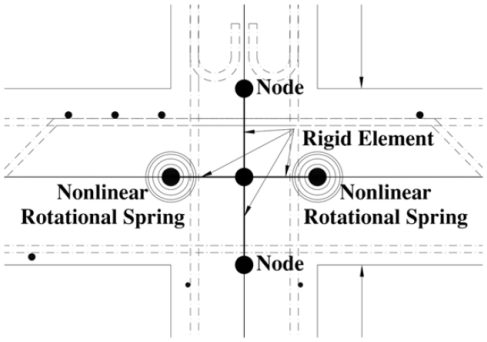

b) Interior joint.

Fig. 5. Proposed model for the exterior and interior substructures reinforced by plain bars [22].

Table 1. Plastic deformations of the spring proposed for modeling of beam-column joints [22].

a (rad)	b (rad)	c (rad)	a' (rad)	b' (rad)
0.009	0.063	0.264	0.166	0.215

The comparison between numerically predicted responses with corresponding experimental outcomes result in the proposed model has been able to predict the capacity of the substructures relatively well [22].

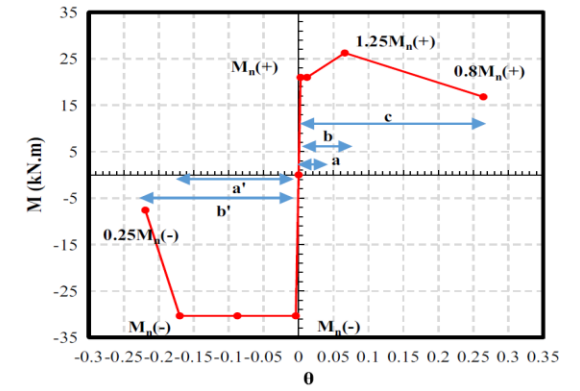

a) Exterior joint.

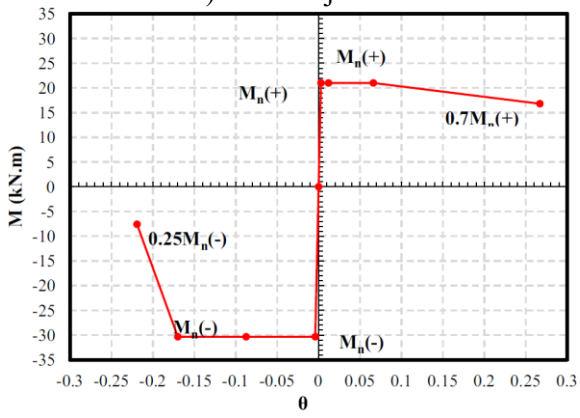

b) Interior joint.

Fig. 6. Properties of the nonlinear rotational spring for the exterior and interior substructures [22].

4. Nonlinear dynamic analysis

4.1. Time-history analysis

In this section, the seismic response of the old 3-story concrete building reinforced by plain bars and represented in this study were investigated due to time-history analysis. The grand motion considered in this study is unscaled Kocaeli earthquake in Turkey. The magnitude and the PGA of this earthquake were 7.5 M_n and 0.22 g respectively (see Fig. 7(a)). The effects of vertical mass irregularity on time-history of base shear, floor displacements and maximum interstory drift ratio of the whole structure are investigated and compared.

Based on Fig. 7(b), variation of base shears from the bottom to the top level of the building, follows increase in each irregularity pattern. As shown in Fig. 7(c) and Fig. 7(d), the story drifts and floor displacement of the buildings increases due to vertical mass irregularity. The average of the increase at floor displacements of the stories in E-W (longitudinal) direction for the buildings with different irregularity including irregular mass located at bottom (IRCP-B), median (IRCP-M), and top story (IRCP-T) are %8.46, %15.06, and %5.32, respectively.

Also, the average of the increase at floor displacements of the stories in N-S (transverse) direction for the buildings with different irregularity including irregular mass located at bottom, median, and top story are %9.21, %24.89 and %26.66, respectively. On average for E-W and N-S direction, the increase at Max inter story drift ratios for the buildings with different irregularity including irregular mass located at bottom (IRCP-B), median (IRCP-M), and top story (IRCP-T) are %7.32, %13.71 and %9.34, respectively. It is important to be noted that irregularity in bottom story has the least effect on the increase of the lateral drift. According to Figure 7(d), the represented buildings are still primarily linear elastic considering the levels of inter story drifts that are less than 0.7%. It happens in concrete structures reinforced by

plain bars due to some reasons such as slippage of the bars in the panel joint of beam-column connections. It causes the yielding deformation of the structural behavior of beam-column joint increased in comparison to the concrete joints reinforced by deformed bars [42].

4.2. Incremental dynamic analysis

Incremental dynamic analyses of the old 3-story concrete building reinforced by plain bars and represented in this study was conducted to develop fragility curves for various damage states. In IDA, a structural model is subjected to a set of ground motion records, scaled to different levels of intensity to describe the structural behavior from elastic to collapse [23][43], [44]. A damage limit state is defined as a threshold condition of buildings corresponding to a certain level of damage under an earthquake. To drive fragility curves, it is necessary to define an Engineering Demand Parameter (EDP) that can be correlated well with damage states. The inter-story-drift ratio is one of the most important EDPs that can predict damage states ranging from slight to destruction of buildings well. In this paper, the provisions of HAZUS-MH-MR-5 was used to determine the average inter story drift ratio corresponding to various damage states [24]. Results of the incremental dynamic analysis are sensitive to ground motion records selected for analyzing the models. Magnitude, source-to-site distance, and soil type are parameters influencing the ground motion record characteristic. To avoid bias in the results, the records of earthquakes were compiled in a way that their magnitudes and source-to-site distances follow the normal distribution [45]. As shown in Fig. 8, histogram curves of magnitude and closest distance to fault rupture variables are approximately well fitted with the normal distribution. The earthquake record set are shown in Table 2.

Incremental dynamic analysis of the existing building, subjected to seismic excitations in two orthogonal directions simultaneously, was conducted under two abovementioned record sets.

The stronger component of each ground motion pair (E-W (longitudinal) direction) was applied along the direction corresponded to the first structural period of the structure. The 5% damped pseudo spectral acceleration at the first mode period of the building, $S_a(T_1)$, was used as the intensity measure to scale the stronger component of each record pair to various intensities. The same scaling factors were used for the weaker components of the time histories to preserve the recorded relationship between the components. The parameter of $S_a(T_1)$ was used for scaling the records because of having two important characteristics of sufficiency and efficiency, particularly for short and moderate-period buildings [47]–[49]. Additionally, seismic hazard curves in terms of $S_a(T_1)$ are available in most regions of the world. For each pair of the records, the intensity was increased until numerical non-convergence is observed or reaching to level of lateral drift in HAZUS, indicating global dynamic instability. The structural response parameter used as the EDP (Engineering Demand Parameters) in this study, is the maximum inter story drift. Fig. 9 shows IDA curves for the non-code-conforming 3-story RC Building with plain bars in E-W (longitudinal) and N-S (transverse) directions. Fig. 10 shows 50% fractile of IDA analysis results for different types of mass irregularity and E-W, N-S directions. To summarize the IDA curves into, 50% fractile

curves, stripes of IM-values were calculated at several levels of the EDP, and the 50% fractile IM values given the EDP-level were estimated. The 50% fractile curves were used to determine the ultimate capacity of the RC existing buildings. The ultimate capacity refers to the capacity at which the local slope of the IDA curve reaches zero. As it was seen in Fig. 10(a), mean of complete collapse capacity of the buildings for E-W (longitudinal) direction and regular mass (RCP), irregular bottom story (IRCP-B), irregular median story (IRCP-M) and irregular top story (IRCP-T) has been evaluated 0.65g, 0.4g, 0.33g and 0.42g, respectively. According to HAZUS, complete collapse capacity of the building refer to the condition which max drift ratio of the story exceeds from 0.04 (see Table. 3) Also, according to Fig.10(b), mean of complete collapse capacity of the buildings N-S (transverse) direction and regular mass (RCP), irregular bottom story (IRCP-B), irregular median story (IRCP-M) and irregular top story (IRCP-T) has been evaluated 0.7g, 0.45g, 0.4g and 0.5g, respectively.

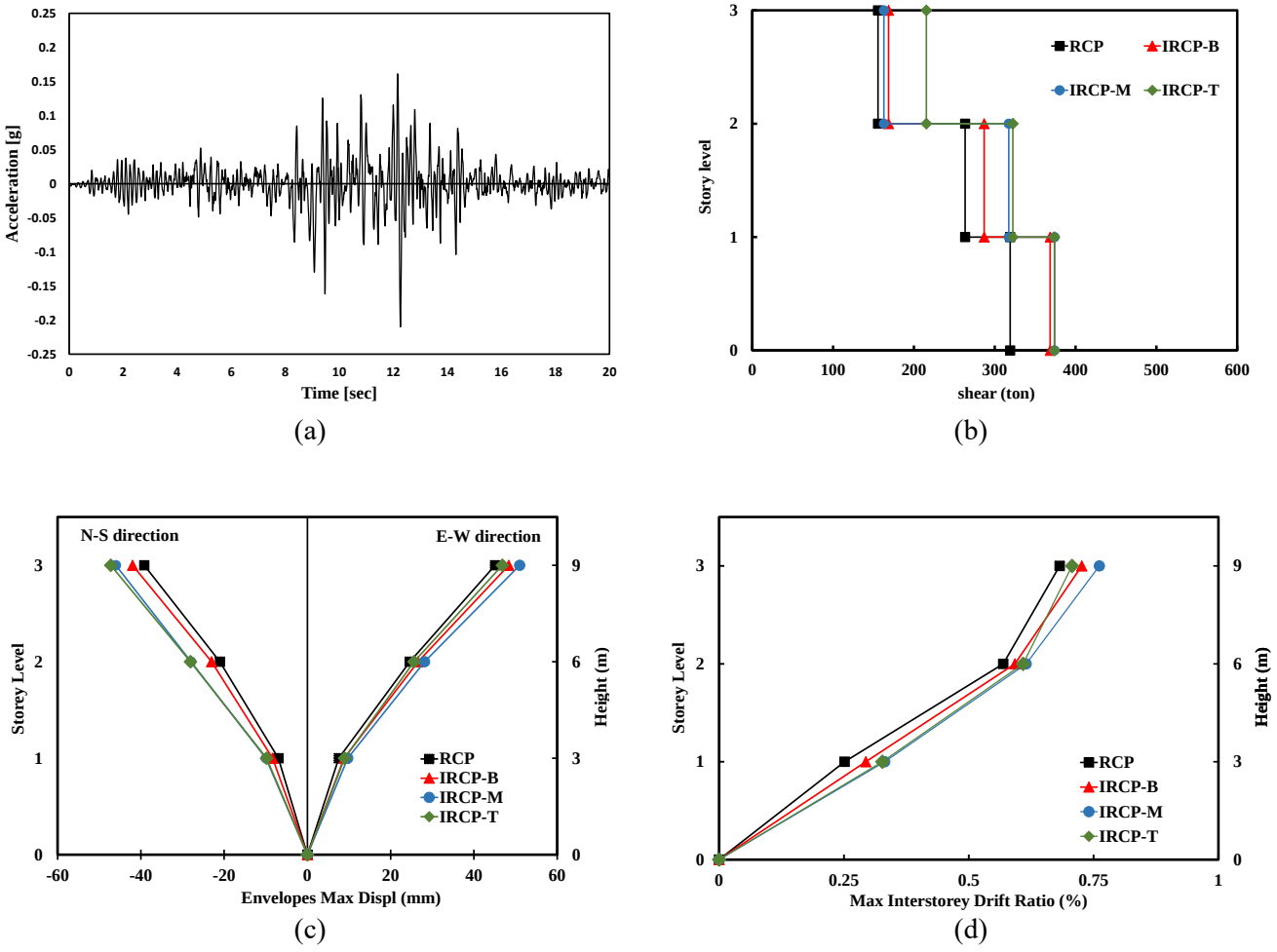

Fig. 7. Comparison of time-history responses of old reinforced concrete building with plain bars under Kocaeli, Turkey earthquake (a) Acceleration time history of Kocaeli, Turkey earthquake (b) base shear (c) floor displacement (d) Max inter story drift ratio (%).

Table 2. Details of 20 earthquake ground motions considered in this study [46].

Far-Field Record Set						
No	Event	Year	Station Name	M	R(Km)	Vs30 (m/s2)
1	Hector Mine	1999	Hector	7.1	11.7	685.00
2	Kobe, Japan	1995	Nishi-Akashi	6.9	7.1	609.00
3	Kocaeli, Turkey	1999	Arcelik	7.5	13.5	523.00
4	Manjil, Iran	1990	Abbar	7.4	12.6	724.00
5	Chi-Chi, Taiwan	1999	TCU045	7.6	26.0	705.00
6	Friuli, Italy	1976	Tolmezzo	6.5	15.8	425.00
7	Tabas	1978	Deyhook	7.4	13.9	471.53
8	Whittier Narrows-01	1987	San Gabriel-E Grand Av	5.9	15.2	401.37
9	Parkfield	1966	Temblor Pre1969	6.1	15.9	527.92
10	Victoria, Mexico	1980	Cerro Prieto	6.3	14.3	471.53
Near Fault Record Set With Pulse						
11	Cape Mendocino	1992	Petrolia	7.0	8.2	713.00
12	Landers	1992	Lucerne	7.3	2.2	685.00
13	Northridge-01	1994	Sylmar - Olive View	5.3	9.0	441
14	Chi-Chi, Taiwan	1978	TCU102	7.6	7.7	714
15	Bam	2003	Bam	6.5	0.0	487.4
Near Fault Record set Without Pulse						
16	Gazli, USSR	1976	Karakyr	6.8	5.5	660
17	Nahanni, Canada	1985	Site 2	6.8	4.9	660
18	Loma Prieta	1989	Corralitos	6.9	3.9	462
19	Cape Mendocino	1992	Cape Mendocino	7.0	7.0	514
20	Silakhor	2006	Chalan Choolan	5.9	9.0	428

Note: The record set includes 20 pairs of horizontal ground motion records, 40 individual components, selected from record sets proposed by the FEMA P695 [46]. Slight changes were made to the FEMA record sets to correspond with the condition of the soil type II Iranian seismic code (2800 code).

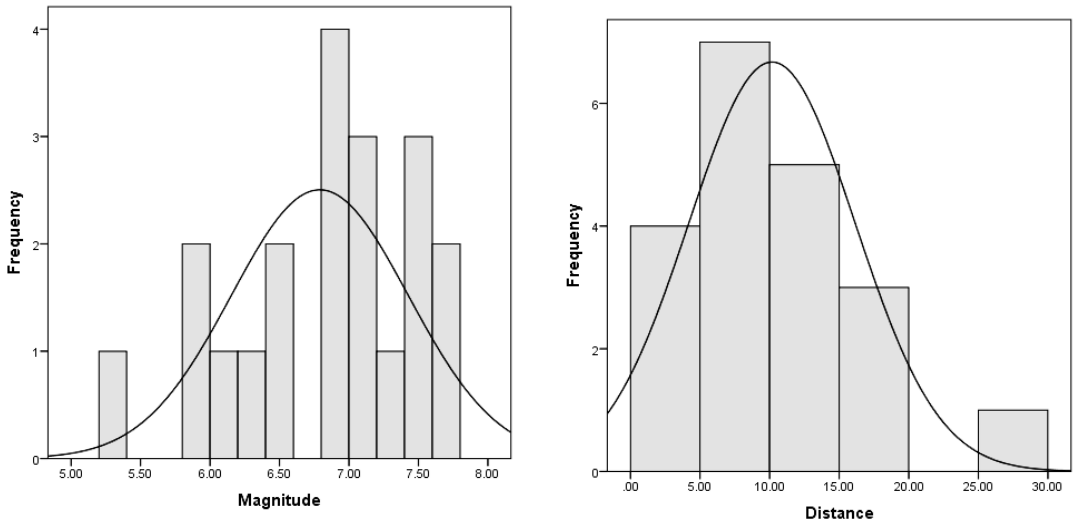

(a) (b)

Fig. 8. Histogram with normal distribution curve for a magnitude, and b closest distance from source-to-site variables.

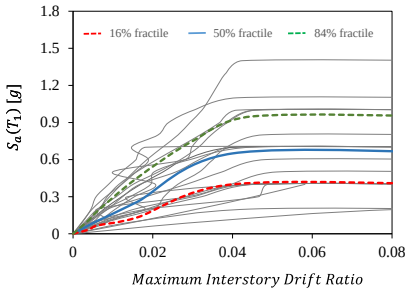

(a) regular (RCP) – E-W direction.

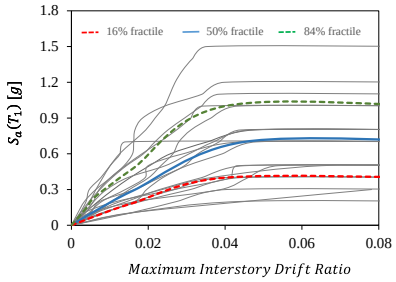

(b) regular (RCP) – N-S direction.

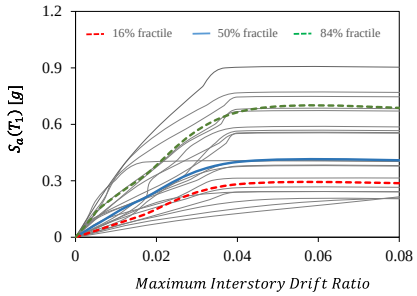

(c) irregular bottom story (IRCP-B) – E-W direction.

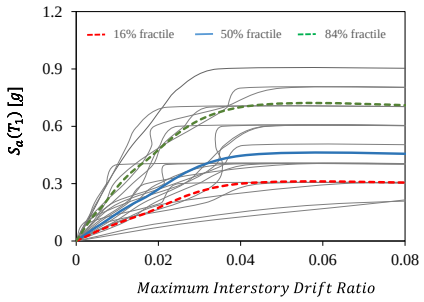

(d) irregular bottom story (IRCP-B) – N-S direction.

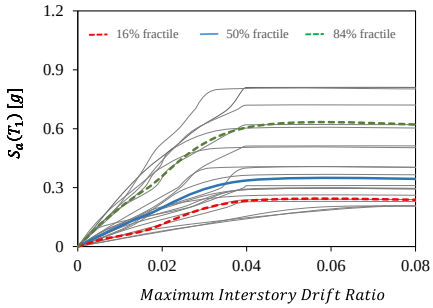

(e) irregular median story (IRCP-M) – E-W direction.

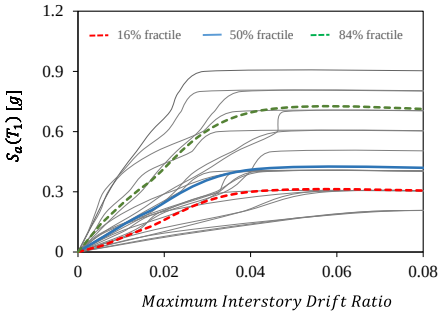

(f) irregular median story (IRCP-M) – N-S direction.

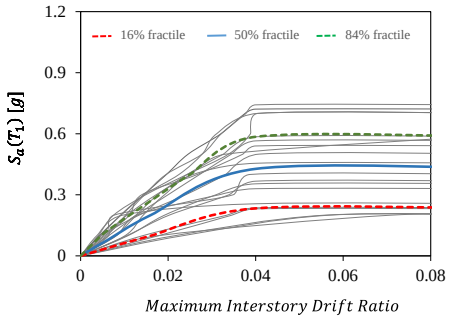

(g) irregular top story (IRCP-T) – E-W direction.

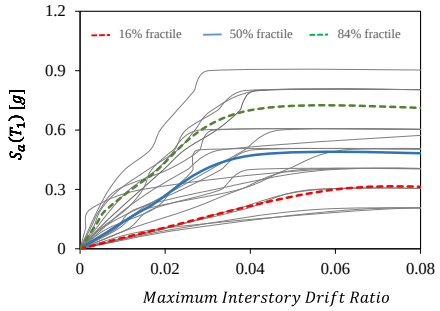

(h) irregular top story (IRCP-T) – N-S direction.

Fig. 9. IDA curves of four RC existing buildings in E-W (longitudinal) directions and N-S (transverse) directions.

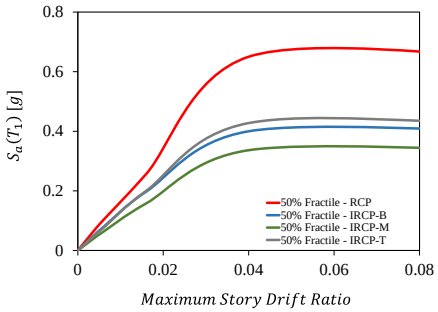

(a) E-W direction.

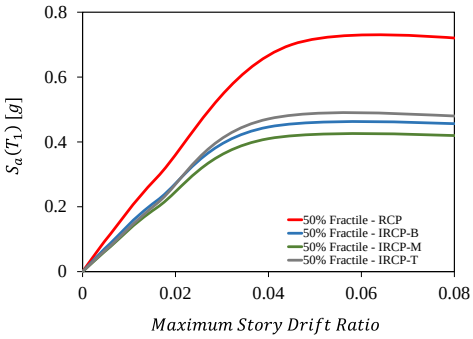

(b) N-S direction.

Fig. 10. Comparison of IDA results for both of E-W (longitudinal) and N-S (transverse) directions.

Table. 3. Inter-story drift ratio for various structural damage states [24].

	Structural Damage States			
	Slight	Moderate	Extensive	Complete
3-story	0.004	0.006	0.016	0.04

5. Development of fragility curves

Considering the lognormal distribution for $S_{a,c}$ values, the fragility function is described in Eq. (2). [50]–[54].

$$P\left(S_{a,c} \le s_a\right) = \phi\left(\frac{\ln(s_a) - \mu_{Ln(S_{a,c})}}{\sigma_{Ln(S_{a,c})}}\right) \quad \text{Eq. (2)}$$

Where ϕ is the standard normal cumulative distribution function, $\mu_{Ln(S_{a,c})}$ is the mean value of the natural logarithm of the damage state capacities, and $\sigma_{Ln(S_{a,c})}$ is the record to record dispersion (i.e., the standard deviation of the natural logarithm of the damage state capacities).

Fig. 11 shows the lognormal distribution fitted to the damage state capacities obtained from the IDA curves. These curves are fragility functions for the non-code-conforming 3-story concrete building reinforced by plain bars with consideration of regularity and irregularity of vertical mass distribution. According to the results, there are considerable differences between the fragility curves developed for building with regular and irregular mass distribution under earthquake ground motions recorded in E-W and N-S directions.

As shown in Fig. 11(a) and Fig. 11(b), by changing the direction E-W to N-S, mean of complete collapse capacity of the represented building for regular mass (RCP), irregular bottom story (IRCP-B), irregular median story (IRCP-M) and irregular top story (IRCP-T) have been decreased %7.69, %12.5, %21.21, and %19.04, respectively.

Fig. 12 provides the median and standard deviation of the fitted lognormal distribution for collapse damage states of the non-code-conforming 3-story concrete building reinforced by plain bars.

On average in E-W direction, considering the effects of vertical mass irregularity, the median capacity of the buildings with mass irregularity at the bottom (IRCP-B), median (IRCP-M), and top story (IRCP-T) compare to the building with regular mass (RCP) distribution are reduced by amount of %38.46, %49.23 and %35.38, respectively. Also for N-S direction, median capacity of the buildings at the bottom, median, and top story compare to the building with regular mass (RCP) distribution are reduced by amount of %37.71, %42.85 and %28.57, respectively.

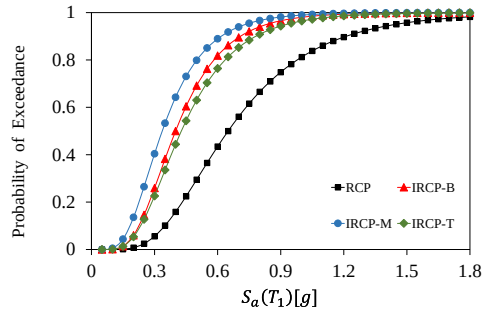

(a) E-W direction.

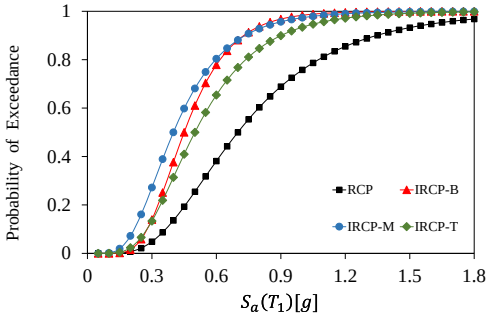

(b) N-S direction

Fig. 11. Fragility curves of the presented RC existing buildings in E-W (longitudinal) and N-S (transverse) directions at complete collapse damage states with consideration of vertical mass irregularity.

For estimating the collapse fragility of the buildings at the MCE level of shaking, at first S_a corresponding to the MCE level should be calculated from the risk analysis curve, and after that we can reach to the probability of exceedance for MCE level of shaking. Fig.13 provides the probability of the complete damage of the represented buildings, given the return period 475 years and 2475 years spectral accelerations of Bojnord city. According to Fig. 13, at spectra acceleration of Bojnord with a return period of 2475 years, complete damage probability in E-W direction of the building with regular mass (RCP), irregular bottom story (IRCP-B), irregular median story (IRCP-M) and irregular top story (IRCP-T) are about %75, %96, %98 and %94, respectively.

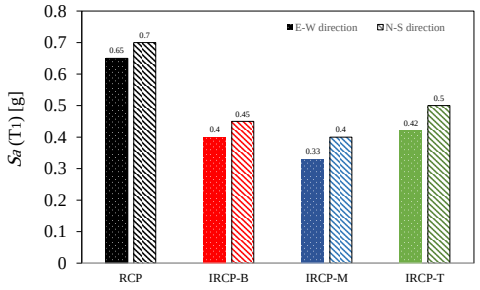

(a) Median of the fitted lognormal distribution.

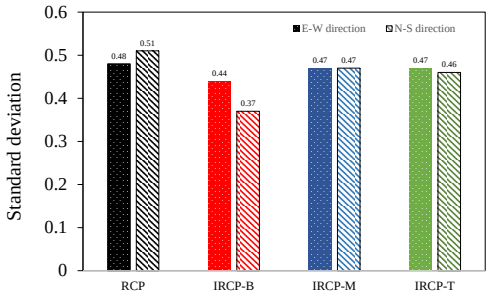

(b) Standard deviation of the fitted lognormal distribution.

Fig. 12.median and standard deviation of the fitted lognormal distribution for collapse damage states.

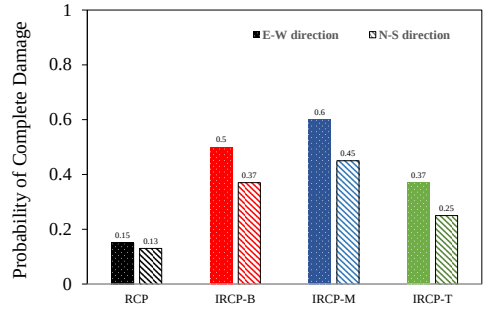

a) return period of 475.

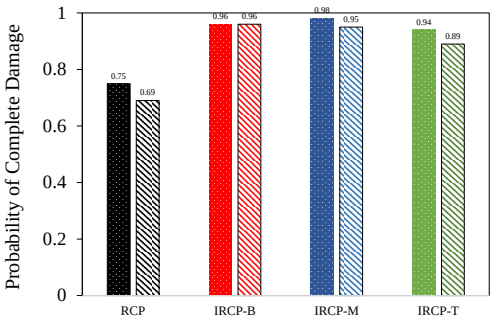

b) return period of 2475.

Fig. 13. Damage probability of various buildings under the earthquake with a return period of 475 years and 2475 years.

6. Hazard and reliability analysis

The probability of exceeding (P_f) a given limit state in a reference time period (in years) was evaluated by reliability analysis due to integrating the convolution of structural fragility curves and hazard curves [30]. A specific fragility curve represents the probability of a specific structure of period T_1 to exceed a specified limit state, and the hazard curve describes the probability of exceeding the intensity $S_a(T_1)$, in a specific site in the reference service time period (Δt). The probability of exceeding a limit state in the reference period (P_f) can be expressed as:

$$P_f = \int P\,[C \ll D|IM = x]P[x]dx \qquad \text{Eq.(3)}$$

where $P[x]$ is the probability of exceeding an IM = x =$S_a(T_1)$, in a specific site in the reference period (50 years) described by a Poisson model as:

$$P[x] = 1 - e^{\lambda[x]\,\Delta t} \qquad \text{Eq.(4)}$$

in which $\lambda[x]$ is a function describing the annual rate of exceeding the IM = x =$S_a(T_1)$. Hazard curves are obtained in a simplified way from spectral ordinates at different vibration periods ($S_a(T_{1,i})$). It can be calculated for different return period (T_R) spectra, associated with the respective annual rates of exceedance ($\lambda = 1/T_R$). The interpolation of results allows determining the hazard curves which are site and period dependent. The convolution integral in Eq. (3) is used to determine the probability of failure (generally intended as the probability of exceeding a limit state) which takes into account both fragility and hazard.

In the present study, we used the results of probabilistic seismic hazard analysis (PSHA) of Bojnord city located in the northeast of Iran [55], [56]. Hazard curves, representing the annual rates of exceeding the IM = x =$S_a(T_1)$ (Fig. 14(a)), are obtained for each vibration period associated with the four structural typologies. Hazard curves are then converted into probabilities of exceedance within a service life of 50 years by using the Poisson's model equation provided in Eq.(4), where is ΔT indeed 50 years and λ [x = IM] the interpolation function for each period. Hazard curves in 50 years for each vibration period are depicted in Fig. 14(b).

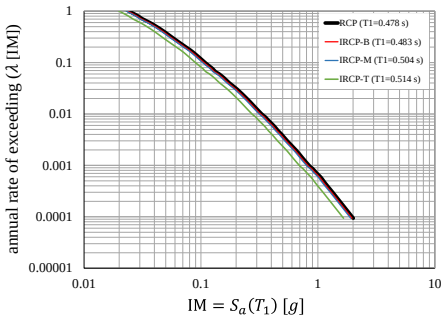

(a)

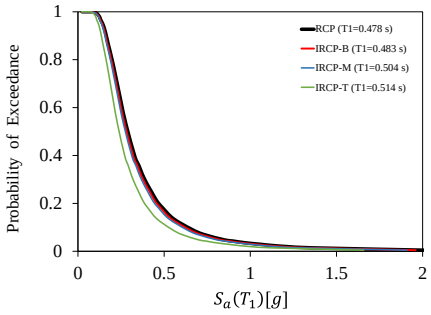

(b)

Fig. 14. Hazard analysis for Bojnord (Iran) (a) annual rate of exceedance curves for different T1 values (b) Probability of exceedance in 50 years curves [55], [56].

In Fig. 15, the hazard curves for the reference vibration periods, are superimposed with fragility curves of the four structural typologies. The intersection areas between hazard and fragility curves are proportional to the probabilities of exceedance the different limit states, which are numerically

determined by Eq.(4). This results can be compared with the outcomes of fragility curves, which have shown better performance of the building with regular mass distribution. The obtained probabilities of occurrence (P_f) for complete damage limit states are compared as bar charts in Fig. 16. This result shows a dramatically increased probability of occurrence of complete damage limit state in the cases of irregular mass distribution. Probabilities of occurrence for irregular bottom (IRCP-B), median (IRCP-M), and top story (IRCP-T) are about 1.51, 1.6, and 1.04 times of the probability of exceedance evaluated for the building with regular mass (RCP) distribution.

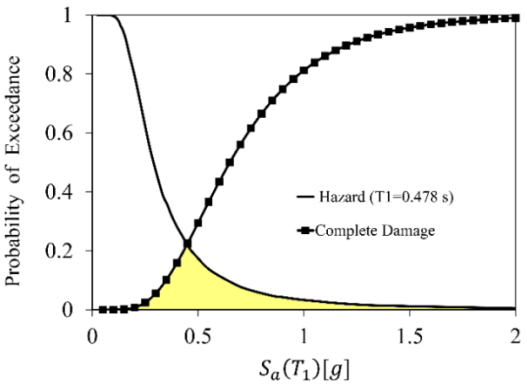

(a) regular (RCP).

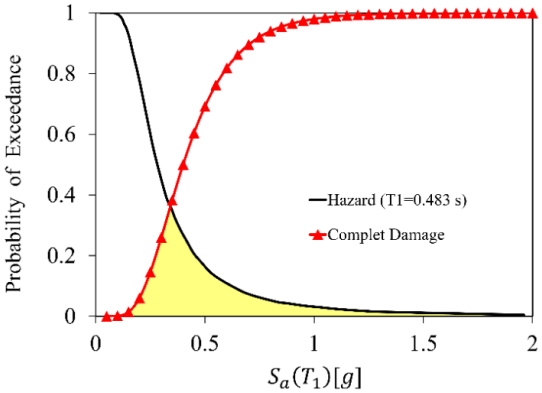

(b) irregular bottom story (IRCP-B).

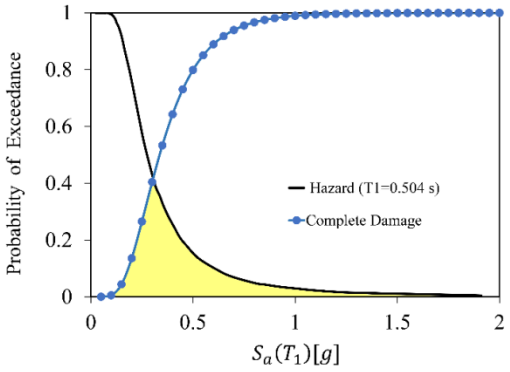

(c) irregular median story (IRCP-M).

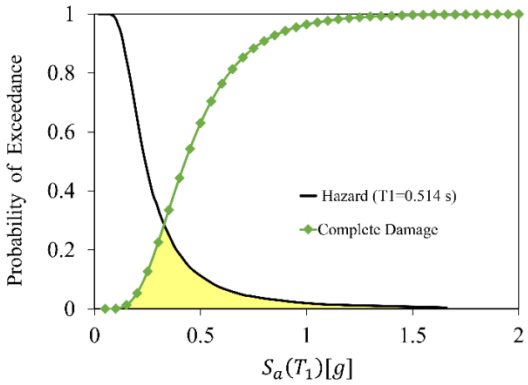

(d) irregular top story (IRCP-T).

Fig. 15. Fragility curves of collapse limit states and hazard curves (Bojnord, Iran) for different irregularity of mass distribution.

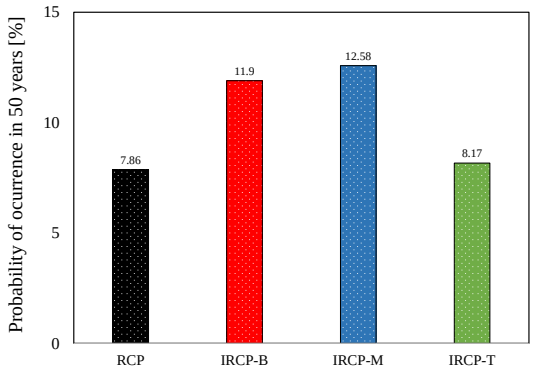

Fig. 16. Probabilities of occurrence in 50 years of collapse limit states by consideration vertical mass irregularity.

7. Conclusion

In this research, Effects of vertical mass irregularity on collapse capacity of the non-code-conforming and existing concrete building reinforced by plain bars were evaluated. The represented building was a three story building constructed before the 1970s and according to the old design codes and references. Damage mode of the structures and behavior of the beam-column joints were considered in the modeling of the structure. Incremental dynamic analyses (IDA) were conducted on the building model using 20 pairs of normalized earthquake records set to develop the fragility curves. Seismic risk assessment allowed comparing the performances of the systems by accounting for both fragility and hazard curves to obtain probabilities of occurrence of complete collapse limit state. The obtained outcomes can be summarized as follows:

Irregular distribution of mass in the height of the building increases the fundamental period of the structure.

All of vertical mass irregularities in different stories cause to increase the time-history of base shear, floor displacements and maximum inter-story drift ratio of the existing RC building.

On average, considering the effects of vertical mass irregularity, the median capacity of the buildings with mass irregularity at the bottom, median, and top story compare to the building with regular mass distribution are reduced by amount of %38.08, %46.04 and %31.97, respectively.

Probabilities of occurrence for irregular bottom, median, and top story are about 1.51, 1.6, and 1.04 times of the probability of exceedance evaluated for the building with regular mass distribution.

References

[1] ASCE7-16., "Minimum design loads for buildings and other structures," *Am. Soc. Civ. Eng. Reston, Virginia.* , 2017.

[2] Standard.No.2800, "Iranian Code of Practice for Seismic Resistant Design of Buildings," *4th Ed. Road, Hous. Urban Deve;opment Res. Center, Tehran, BHRC-PN S-253*, 2014.

[3] FEMA P-2012, "Assessing Seismic Performance of Buildings with Configuration Irregularities, Calibrating Current Standards and Practices," 2018.

[4] E. V Valmundsson and J. M. Nau, "Seismic response of building frames with vertical structural irregularities," *J. Struct. Eng.*, vol. 123, no. 1, pp. 30–41, 1997.

[5] Al-Ali, K. A.A., and H. Krawinkler, "Effects of vertical irregularities on seismic behaviour of building structures. ," *Rep. No. 130. Dep. Civ. Environ. Eng. Stanford Univ. San Fr.*, 1998.

[6] B. J. Choi, "Hysteretic energy response of steel moment-resisting frames with vertical mass irregularities," *Struct. Des. Tall Spec. Build.*, vol. 13, no. 2, pp. 123–144, 2004.

[7] M. DeStefano, E. M. Marino, and S. Viti, "Evaluation of second order effects on the seismic response of vertically irregular RC framed structures," *Proc. 4th Eur. Work.*

Seism. Behav. Irregul. complex Struct. Thessaloniki, Greece, 2005.

[8] F. Michalis, V. Dimitrios, and P. Manolis, "Evaluation of the influence of vertical irregularities on the seismic performance of a nine-storey steel frame," *Earthq. Eng. Struct. Dyn.*, vol. 35, no. 12, pp. 1489–1509, 2006.

[9] T. L. Karavasilis, N. Bazeos, and D. E. Beskos, "Estimation of seismic inelastic deformation demands in plane steel MRF with vertical mass irregularities," *Eng. Struct.*, vol. 30, no. 11, pp. 3265–3275, 2008.

[10] M. Pirizadeh and H. Shakib, "Probabilistic seismic performance evaluation of non-geometric vertically irregular steel buildings," *J. Constr. Steel Res.*, vol. 82, pp. 88–98, 2013.

[11] A. Habibi and K. Asadi, "Seismic performance of RC frames irregular in elevation designed based on Iranian seismic code," *J. Rehabil. Civ. Eng.*, vol. 1, no. 2, pp. 40–55, 2013.

[12] V. Mohsenian and A. Nikkhoo, "A study on the effects of vertical mass irregularity on seismic performance of tunnel-form structural system," *Adv. Concr. Constr.*, vol. 7, no. 3, pp. 131–141, 2019.

[13] M. Amiri and M. Yakhchalian, "Performance of intensity measures for seismic collapse assessment of structures with vertical mass irregularity," *Structures*, vol. 24, pp. 728–741, 2020.

[14] A. Karami, S. Shahbazi, and M. Kioumarsi, "A study on the effects of vertical mass irregularity on seismic behavior of BRBFs and CBFs," *Appl. Sci.*, vol. 10, no. 23, p. 8314, 2020.

[15] K. Ghimire and H. Chaulagain, "Influence of structural irregularities on seismic performance of RC frame buildings," *J. Eng. Issues Solut.*, vol. 1, no. 1, pp. 70–87, 2021.

[16] Y. Bai, Y. Li, Z. Tang, M. Bittner, M. Broggi, and M. Beer, "Seismic collapse fragility of low-rise steel moment frames with mass irregularity based on shaking table test," *Bull. Earthq. Eng.*, vol. 19, no. 6, pp. 2457–2482, 2021.

[17] L. Halder and S. Paul, "Seismic damage evaluation of gravity load designed low rise RC building using non-linear static method," *Procedia Eng.*, vol. 144, pp. 1373–1380, 2016.

[18] K. K. Arani, M. S. Marefat, A. Amrollahi-Biucky, and M. Khanmohammadi, "Experimental seismic evaluation of old concrete columns reinforced by plain bars," *Struct. Des. Tall Spec. Build.*, vol. 22, no. 3, pp. 267–290, 2013.

[19] M. Adibi, M. S. Marefat, A. Esmaeily, K. K. Arani, and A. Esmaeily, "Seismic retrofit of external concrete beam-column joints reinforced by plain bars using steel angles prestressed by cross ties," *Eng. Struct.*, vol. 148, 2017, doi: 10.1016/j.engstruct.2017.07.014.

[20] M. Adibi, M. S. Marefat, K. K. Arani, and H. Zare, "External retrofit of beam-column joints in old fashioned RC structures," *Earthq. Struct.*, vol. 12, no. 2, 2017, doi: 10.12989/eas.2017.12.2.237.

[21] M. Adibi and R. Talebkhah, "Development of seismic fragility curves for the existing RC building with plain bars," *Eur. J. Environ. Civ. Eng.*, pp. 1–16, 2020.

[22] M. Adibi, M. S. Marefat, and R. Allahvirdizadeh, "Nonlinear modeling of cyclic response of RC beam–column joints reinforced by plain bars," *Bull. Earthq. Eng.*, 2018, doi: 10.1007/s10518-018-0399-4.

[23] D. Vamvatsikos and C. A. Cornell, "Incremental dynamic analysis," *Earthq. Eng. Struct. Dyn.*, vol. 31, no. 3, pp. 491–514, 2002, doi: https://doi.org/10.1002/eqe.141.

[24] HAZUS-MH MR5, "Earthquake loss Estimation Methodology Model," *FEMA, Washington, D.C*, 2005.

[25] S. B. Kadam, Y. Singh, and L. Bing, "Seismic fragility reduction of an unreinforced masonry school building through retrofit using ferrocement overlay," *Earthq. Eng. Eng. Vib.*, vol. 19, pp. 397–412, 2020.

[26] S. Ahmad, N. Kyriakides, K. Pilakoutas, K. Neocleous, and Q. uz Zaman, "Seismic fragility assessment of existing sub-standard low strength reinforced concrete structures," *Earthq. Eng. Eng. Vib.*, vol. 14, no. 3, pp. 439–452, 2015.

[27] R. K. L. Su and C.-L. Lee, "Development of seismic fragility curves for low-rise masonry infilled reinforced concrete buildings by a coefficient-based method," *Earthq. Eng. Eng. Vib.*, vol. 12, no. 2, pp. 319–332, 2013.

[28] A. Abo-El-Ezz, M.-J. Nollet, and M. Nastev, "Seismic fragility assessment of low-rise stone masonry buildings," *Earthq. Eng. Eng. Vib.*, vol. 12, no. 1, pp. 87–97, 2013.

[29] J. Ren, J. Song, and B. R. Ellingwood, "Reliability assessment framework of deteriorating reinforced concrete bridges subjected to earthquake and pier scour," *Eng. Struct.*, vol. 239, p. 112363, 2021.

[30] F. Di Trapani, V. Bolis, F. Basone, and M. Preti, "Seismic reliability and loss assessment of RC frame structures with traditional and innovative masonry infills," *Eng. Struct.*, vol. 208, p. 110306, 2020.

[31] F. W. Taylor, S. E. Thompson, and E. Smulski, "Concrete, Plain and Reinforced," *J. Wiley sons, Inc.*, vol. 4, 1925.

[32] C. W. Duhman, "The theory and practice of reinforced concrete," *McGraw-Hill, New York*, 1953.

[33] P. Pernot, "Le béton armé," *JB Baillière*, 1954.

[34] A. Guerrin, "Traite De Beton Arme," *Dunod, Paris*, 1959.

[35] J. A. Barker, "Reinforced concrete detailing," *Oxford Univ. Press. London (1st Print. 1967)*, vol. vol Second, 1979.

[36] N. J. Edvard and J. L. Tanner, "Theory and problems of reinforced concrete design," *Schaum Publ. co., New York*, 1996.

[37] Opensees, "Open system for earthquke engineering simulation, Pacific Earthquake Engineering Research Center, University of Califonia, Brekely Ca, http://opensees.berkeley.edu/," 2016.

[38] L. Petrini, C. Maggi, M. J. N. Priestley, and G. M. Calvi, "Experimental verification of viscous damping modeling for inelastic time history analyzes," *J. Earthq. Eng.*, vol. 12, no. S1, pp. 125–145, 2008, doi: http://doi.org/10.1080/13632460801925822.

[39] J. F. Hall, "Problems encountered from the use (or misuse) of Rayleigh damping," *Earthq. Eng. Struct. Dyn.*, vol. 35, no. 5, pp. 525–545, 2006, doi: https://doi.org/10.1002/eqe.541.

[40] M. Adibi, R. Talebkhaha, and A. Yahyaabadib, "Simulation of cyclic response of precast concrete beam-column joints," *Comput. Concr.*, vol. 24, no. 3, 2019, doi: 10.12989/cac.2019.24.3.223.

[41] M. Adibi, R. Talebkhah, and A. Yahyaabadi, "Nonlinear modeling of exterior beam-column joints in precast concrete buildings," *J. Struct. Constr. Eng.*, 2020.

[42] M. Adibi, J. Shafaei, and F. Aliakbari, "Experimental evaluation of external beam-column joints reinforced by deformed and plain bar," *EARTHQUAKES Struct.*, vol. 18, no. 1, pp. 113–127, 2020.

[43] D. Vamvatsikos and C. A. Cornell, "The incremental dynamic analysis and its application to performance-based earthquake engineering," *Proc. 12th Eur. Conf. Earthq. Eng.*, 2002.

[44] D. Vamvatsikos and A. Cornell, "Incremental dynamic analysis with two components of motion for a 3D steel structure," 2006.

[45] M. Javanmard and A. Yahyaabadi, "Assessment of Structure-Specific Intensity Measures for the Probabilistic Seismic Demand Analysis of Steel Moment Frames," *Arab. J. Sci. Eng.*, vol. 44, no. 5, pp. 4885–4894, 2019.

[46] FEMA P695, "Quantification of building seismic performance factors," *Fed. Emerg. Manag. Agency, Washington, D.C*, 2009.

[47] M. Onvani and A. Yahyaabadi, "Probabilistic seismic demand analysis of steel moment frames by utilising Bayesian

statistics," *Eur. J. Environ. Civ. Eng.*, pp. 1–17, 2018.

[48] N. Shome, C. A. Cornell, P. Bazzurro, and J. E. Carballo, "Earthquakes, records, and nonlinear responses," *Earthq. Spectra*, vol. 14, no. 3, pp. 469–500, 1998.

[49] L. Ye, Q. Ma, Z. Miao, H. Guan, and Y. Zhuge, "Numerical and comparative study of earthquake intensity indices in seismic analysis," *Struct. Des. Tall Spec. Build.*, vol. 22, no. 4, pp. 362–381, 2013.

[50] F. Izanlu and A. Yahyaabadi, "Determination of structural fragility curves of various building types for seismic vulnerability assessment in the Sarpol-e Zahab City," *J. Seismol. Earthq. Eng.*, vol. 20, no. 3, pp. 93–107, 2019.

[51] A. E. Özel and E. M. Güneyisi, "Effects of eccentric steel bracing systems on seismic fragility curves of mid-rise R/C buildings: A case study," *Struct. Saf.*, vol. 33, no. 1, pp. 82–95, 2011.

[52] H. L. Sadraddin, X. Shao, and Y. Hu, "Fragility assessment of high-rise reinforced concrete buildings considering the effects of shear wall contributions," *Struct. Des. Tall Spec. Build.*, vol. 25, no. 18, pp. 1089–1102, 2016.

[53] R. Talebkhah, A. A. Yahyaabadi, and M. Adibi, "Development of fragility curves for precast concrete frames comparing the methods of static pushover and incremental dynamic analysis," *Sharif J. Civ. Eng.*, vol. 36.2, no. 2.1, pp. 129–140, 2020, [Online]. Available: http://sjce.journals.sharif.edu/article_21292_fad849655a81ea736c14dca6d65afbfb.pdf.

[54] M. Adibi, A. Yahyaabadi, and R. Talebkhah, "Seismic behavior assessment of RC precast frame damaged in Bojnord Earthquake 2017 considering soil-structure interaction effects," *Amirkabir J. Civ. Eng.*, vol. 53, no. 7, p. 19, 2021.

[55] M. Rahimi and A. Yahyaabadi, "Bayesian probabilistic seismic hazard analysis with respect to near-fault effects," *Asian J. Civ. Eng.*, vol. 20, no. 3, pp. 341–349, 2019.

[56] F. Nodehi and A. Yahyaabadi, "Probabilistic seismic hazard analysis of Bojnord region by considering near-fault effects," *Pap. Present. 6th Int. Conf. Earthq. Struct. Kerman, Iran*, 2015.